

1 High-resolution global shipping emission inventory by 2 Shipping Emission Inventory Model (SEIM)

3 Wen Yi ¹†, Xiaotong Wang ² †, Tingkun He ¹, Huan Liu ^{1*}, Zhenyu Luo ¹, Zhaofeng Lv
4 ¹, Kebin He ¹

5 ¹ State Key Joint Laboratory of ESPC, School of Environment, Tsinghua University, Beijing 100084,
6 China

7 ² Key Laboratory of Beijing on Regional Air Pollution Control, Beijing University of Technology,
8 Beijing 100124, China

9 *Correspondence to: liu_env@tsinghua.edu.cn (H. Liu)

10 † These authors contributed equally to this work

11 **Abstract:** The high-resolution ship emission inventory serves as a crucial dataset for various disciplines
12 including atmospheric science, marine science, environmental management, etc. Here, we present a
13 global high spatiotemporal resolution ship emission inventory at a resolution of $0.1^\circ \times 0.1^\circ$ for the years
14 2013, 2016-2021, generated by the state-of-the-art Shipping Emission Inventory Model (SEIMv2.2).
15 Initially, the annual 30 billion Automatic Identification System (AIS) data underwent extensive cleaning
16 to ensure data validity and accuracy in temporal and spatial distribution. Subsequently, integrating real-
17 time vessel positions and speeds from AIS data with static technical parameters, emission factors, and
18 other computational parameters, SEIM simulated ship emissions on a ship-by-ship, signal-by-signal basis.
19 Finally, the results were aggregated and analyzed. In 2021, the ship activity dataset established based on
20 AIS data covered 109.3 thousand vessels globally (101.4 thousand vessels reported by the United Nations
21 Conference on Trade and Development). Concerning the major air pollutants and greenhouse gases,
22 global ships emitted 847.2 million tons of CO₂, 2.3 million tons of SO₂, 16.1 million tons of NO_x, 791.2
23 kilo tons of CO, 737.3 kilo tons of HC (Hydrocarbon), 415.5 kilo tons of primary PM_{2.5}, 61.6 kilo tons
24 of BC (black carbon), 210.3 kilo tons of CH₄, 45.1 kilo tons of N₂O in 2021, accounting for 3.2% of SO₂,
25 14.2% of NO_x, and 2.3% of CO₂ emissions from all global anthropogenic sources, based on the
26 Community Emissions Data System (CEDs). Due to the implementation of fuel-switching policies,
27 global ship emissions of SO₂ and primary PM_{2.5} saw a significant reduction of 81.3% and 76.5% in 2021
28 compared to 2019, respectively. According to the inventory results, the composition of vessel types
29 contributing to global ship emissions remained relatively stable through the years, with container ships

30 consistently contributing ~30% of global ship emissions. Regarding vessel age distribution, the emission
31 contribution of vessels built before 2000 (without Tier standard) has been declining, dropping to 10.2%
32 in 2021, suggesting that even a complete phase-out of these vessels would have limited potential for
33 reducing NOx emissions in the short term. On the other hand, the emission contribution of vessels built
34 after 2016 (meeting Tier III standard) kept increasing, reaching 13.3% in 2021. Temporally, global ship
35 emissions exhibited minimal daily fluctuations. Spatially, high-resolution emission characteristics of
36 different vessel types were delineated. Patterns of ship emission contributions by different types of
37 vessels vary among maritime regions, with container ships predominant in the North and South Pacific,
38 bulk carriers predominant in the South Atlantic, and oil tankers prevalent in the Arabian Sea. The
39 distribution characteristics of ship emissions and intensity also vary significantly across different
40 maritime regions. Our dataset, which is accessible at <https://zenodo.org/records/11069531> (Wen et al.,
41 2024), provides daily breakdown by vessel type and age is available for broad research purposes, and it
42 will provide a solid data foundation for fine-scale scientific research and shipping emission mitigation.

43 **1 Introduction**

44 Ships carry over 80% of global trade volume(Development, 2023). Employing heavy fuel oil, ships
45 emit significantly more atmospheric pollutants than diesel cars each year(Corbett et al., 1999; Endresen
46 et al., 2003; Jasper Faber, 2020). Existing studies indicate that ship emissions of atmospheric pollutants
47 and greenhouse gases have important environmental and climatic impacts on multiple spheres of the
48 Earth (Browse et al., 2013; Chen et al., 2020; Diamond, 2023; Zhang et al., 2021). In terms of air quality,
49 ships are regarded as a major source of PM_{2.5} pollution in coastal cities (Liu et al., 2024; Luo et al., 2023).
50 Recent studies show that although ship emissions have decreased due to stricter control measures in
51 recent years, shipping-related mortality associated with long-term PM_{2.5} exposure in Chinese coastal
52 areas increased by 11.4% from 2016 to 2020 as populations migrate towards coastal cities (Luo et al.,
53 2024). Ship emission-induced sulfur oxides aerosols, significantly influence local climates (Liu et al.,
54 2016; Yuan et al., 2022). With the increasing navigation in the Arctic, ship emissions of black carbon
55 have become a focal point of research and policy debates regarding their impact on the polar ice surface
56 (Stephenson et al., 2018; Zhang et al., 2019). Regarding their impact on marine organisms, anthropogenic

57 emissions account for over 80% of the utilizable nitrogen deposition in the ocean, with maritime
58 emissions contributing to 15% of global NO_x emissions (Zhang et al., 2021). Given these facts,
59 characterizing ship emissions is crucial for fundamental research in atmospheric, marine, and climatic
60 sciences, etc.

61 The characterization of ship emissions through emission inventories stands as a pivotal and effective
62 methodology within maritime emissions research (Liu et al., 2016; Liu et al., 2024; Wang et al., 2021).
63 Over the past 30 years, with the improvement of ship activity data collection mechanisms, the
64 establishment of ship emission inventories has gradually shifted from the "top-down" approach, based
65 on fuel or power consumption statistics and empirical parameters, to the "bottom-up" approach, based
66 on high spatiotemporal resolution shipping trajectory data (Eyring et al., 2010; Jasper Faber, 2020; Liu
67 et al., 2016). Currently, the establishment of high spatiotemporal resolution ship emission inventories
68 based on Automatic Identification System (AIS) data has become the most popular tool for scientific
69 research and policy management in the field of ship emissions (Johansson et al., 2017; Kramel et al.,
70 2021; Wang et al., 2021). AIS consists of onboard equipment, shore-based and satellite-based receivers.
71 During navigation, the onboard equipment transmits AIS signals every 2 seconds to several minutes,
72 which are received by terrestrial or satellite-based AIS receivers and then transmitted in-time to servers
73 for storage. AIS messages record the ship's unique identifier and high-frequency dynamic information
74 that changes continuously as the vessel progresses, including the vessel's MMSI code, IMO number,
75 signal transmission time, ship's position (longitude and latitude), over-ground speed, operational status,
76 draft, and destination, among others. Leveraging real-time ship speed derived from AIS data along with
77 vessel technical specifications such as deadweight tonnage and design speed, and emission factors, it is
78 feasible to model instantaneous ship emissions and then aggregate them at a defined spatiotemporal
79 granularity, thereby constructing a high-resolution emission inventory dataset. The advantage of this
80 method is that the derived emission inventory does not rely on external spatiotemporal allocation
81 parameters, but retains accurate spatiotemporal information of ship emissions from AIS data (Liu et al.,
82 2016). However, the challenge lies in the difficulty of processing AIS data, the complexity of simulating
83 instantaneous ship emissions, and the significant computational resources required (Chen and Yang,
84 2024). Currently, the mainstream international ship emission inventory models based on AIS data include
85 the Ship Traffic Emission Assessment Model (STEAM)(Jalkanen et al., 2012; Johansson et al., 2017) ,

86 the Shipping Emission Inventory Model (SEIM), International Maritime Organization (IMO) emission
87 inventory model (Jasper Faber, 2020), Maritime Transport Environmental Assessment Model
88 (MariTEAM) (Kramel et al., 2021), etc.

89 In this study, we established a $0.1^\circ \times 0.1^\circ$ global daily ship emission inventory for the years 2013,
90 2016-2021 based on SEIMv2.2. This dataset covers five air pollutants (NO_x , SO_2 , $\text{PM}_{2.5}$, CO , HC) and
91 four greenhouse gases (CO_2 , CH_4 , N_2O , BC). Due to rigorous quality control, the ship emission inventory
92 established by SEIM possesses high information density, allowing for analysis across multiple
93 dimensions, such as fleet structure and spatiotemporal characteristics. Initially, we conducted meticulous
94 data cleaning and rigorous quality control on the commercially obtained global ship AIS data to establish
95 a reliable ship activity dataset. Subsequently, employing the latest emission factor and real-time engine
96 power simulation methods for ships, SEIMv2.2 computed instantaneous ship emissions, integrating
97 multiple quality control techniques such as interpolation processing for sparse routes and safety margin
98 considerations to ensure the accuracy of ship emission simulation. Finally, we aggregated ship emissions
99 from different temporal and spatial scales, as well as from different types and ages of ships. The derived
100 high-resolution global shipping emission inventory could serve as input data for climate or atmospheric
101 chemistry models.

102 The next section will elucidate the methodology and factors employed in establishing our high-
103 resolution ship emission inventory. Section 3.1 compares our results with previous global ship emission
104 inventories. Section 3.2 analyzes the temporal sequence of global ship emissions. Section 3.3 examines
105 the spatial distribution characteristics of global ship emissions. Section 4 provides information regarding
106 our dataset and data availability. Finally, Section 5 presents the conclusion.

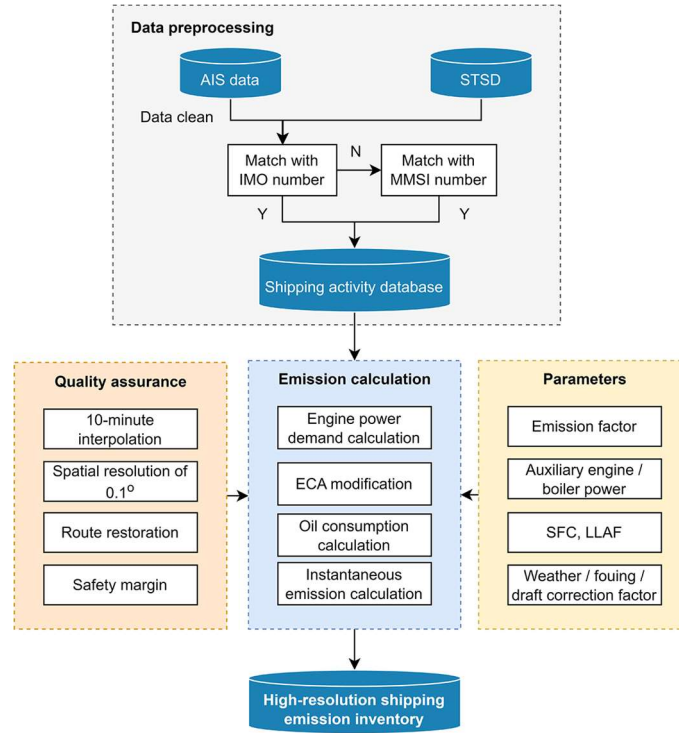
107 **2 Methods**

108 **2.1 Ship Emission Inventory Model (SEIM)**

109 **2.1.1 General principles**

110 The Shipping Emission Inventory Model (SEIM) was first established by (Liu et al., 2016) based on the
111 idea of disaggregated dynamic method. Driven by AIS data, combined with each vessel's registration
112 information, SEIM realized real-time, vessel-by-vessel shipping emission simulations. SEIM is suitable

113 for the establishment of multi-scale shipping emission inventories with applications on regions (Liu et
114 al., 2016; Wang et al., 2021) and ports (Fu et al., 2017). SEIM has undergone two major updates:
115 SEIMv2.0 (Wang et al., 2021) and SEIMv2.2 (this study). Compared to SEIMv2.0, SEIMv2.2 features
116 three key improvements. (1) IMO numbers are employed as the primary identifier to match AIS data and
117 Ship Technical Specifications Database (STSD), and for those that cannot be matched, MMSI (Maritime
118 Mobile Service Identity) codes are used as the secondary identifier. We found that the matching rate of
119 the ship archive database established in previous years could significantly decrease when applied to new
120 years. This is because when ships are leased or AIS equipment is replaced, the MMSI code often changes,
121 while the IMO code remains constant. Therefore, using the IMO code as the first-choice identifier ensures
122 more accurate matching of AIS data and static ship information. See Sect. 2.1.2 for details. (2) The
123 formula for calculating the main engine load has been revised to include parameterized correction
124 schemes for draft, meteorological conditions, and hull fouling. Additionally, a main engine load
125 maximum limit of 98% is set to consider the navigation safety of ships. Refer to Sect. 2.1.3 for further
126 details. (3) The ship emission factors are comprehensively updated according to the Fourth Green House
127 Gases Study by IMO (Jasper Faber, 2020), and a black carbon calculation module has been integrated.
128 This update also integrates the Emission Control Area (ECA) module correction module directly into the
129 calculation process, rather than applying it as a post-process adjustment. Detailed methods are provided
130 in Sect. 2.1.4. During the development of SEIMv2.2, SEIMv2.1 was derived, which only updated the
131 emission factors compared to SEIMv2.0. Generally, the technical scheme of SEIMv2.2 is illustrated in
132 Fig. 1.



133

134 **Figure 1: The technical scheme for SEIMv2.2**

135 The calculation process and principles of SEIMv2.2 could be described as follows: Firstly, the original
 136 AIS data collected are subjected to cleaning, missing data filling, etc., to establish a well-cleaned dynamic
 137 AIS database. Secondly, IMO or MMSI codes are used as unique identifiers to match AIS data with the
 138 STSD, which provides essential technical parameters such as vessel type, deadweight tonnage, main
 139 engine power rating, design speed, etc., to establish a comprehensive shipping activity database. For the
 140 details of STSD, refer to (Wang et al., 2021). This study has incorporated information on newly built
 141 vessels from 2019 to 2021, obtained from the Lloyd's Register, into the established STSD. Thirdly, a
 142 series of parameters such as emission factors, auxiliary engine and boiler output power, specific fuel
 143 consumption, low load adjustment factors, and weather and fouling factors are input for ship emission
 144 simulation. Then, the model will calculate GHGs (Greenhouse gases) and air pollutant emissions for
 145 every ship by every two subsequent AIS signals. The emissions from the main engine, auxiliary engine,
 146 and boiler are simulated using the corresponding formulas presented as Equation (1) - (3).

$$E_{ME,i,n,p} = P_{ME,i,n} \times EF_{ME,i,p} \times LLAF_{i,n,p} \times \Delta T_{i,n} \times 10^{-6} \quad (1)$$

147

$$E_{AE,i,n,p} = P_{AE,i,n} \times EF_{AE,i,p} \times \Delta T_{i,n} \times 10^{-6} \quad (2)$$

148

$$E_{B,i,n,p} = P_{B,i,n} \times EF_{B,i,p} \times \Delta T_{i,n} \times 10^{-6} \quad (3)$$

149 Where the subscripts ME, AE, and B represent the main engine, auxiliary engine, and boiler, respectively;
 150 i represents individual ship; n represents the n -th AIS signals in the sequence, and the total number of
 151 AIS signals transmitted by the ship i could be expressed using N_i ; p represents species of GHGs or air
 152 pollutants. As for the capital letters, E represents the emissions of GHGs or air pollutants (unit: ton); EF
 153 is the emission factors (unit: g/kwh); P is the output power (unit: kw); ΔT is the time interval of two
 154 subsequent AIS signals (unit: h); LLAF is the low load adjust factor, which is applied only when the
 155 main engine load factor is lower than 20%, consistent with our previous work. The total emissions are
 156 calculated by summing up the emissions from all main engines, auxiliary engines, and boilers, as shown
 157 in Equation (4).

$$E_{i,p} = \sum_{n=1}^{N_i-1} E_{i,n,p} = \sum_{n=1}^{N_i-1} (E_{ME,i,n,p} + E_{AE,i,n,p} + E_{B,i,n,p}) \quad (4)$$

158 During the real-time calculation, linear interpolation is applied to latitude and longitude displacement as
 159 well as time intervals where the AIS time interval is greater than ten minutes. AIS latitude and longitude
 160 are rounded to one decimal place to ensure a spatial resolution of $0.1^\circ \times 0.1^\circ$. In the Chinese coastal
 161 region, route restoration technology is applied to restore routes crossing land, referred to (Wang et al.,
 162 2021). If, due to anomalies in speed or other factors, the main engine load exceeds 100%, it is capped at
 163 98% for safety navigation considerations. Finally, the high-resolution emission inventory generated by
 164 SEIM could be aggregated and analyzed from various angles such as emission structure, temporal
 165 variations, spatial distribution, etc., depending on study demands.

166 2.1.2 AIS data cleaning

167 AIS data provide high-density vessel activity data, including time, speed, and latitude-longitude
168 coordinates. This study collected global shore-based and satellite-based AIS data, with an average annual
169 signal count of approximately 30 billion. Due to irregular or erroneous information entry at ports or on
170 vessels, as well as interference from complex marine environments, weather conditions, and terrain, AIS
171 data may suffer from errors, duplicates, and losses. To enhance the accuracy of emission inventory
172 calculations, this study conducted meticulous cleaning of AIS data. Firstly, to ensure data validity, we
173 filter AIS message records that met all of the following conditions: 1) Annual AIS signal count greater
174 than 10; 2) Speed over ground less than 50 knots; 3) Longitudes ranged from -180° to 180° and latitudes
175 ranged from -90° to 90° ; 4) The timestamp of AIS signals within the target year.

176 Secondly, for temporal anomaly cleaning, signals with excessively long time intervals are filtered
177 out. According to the International Convention for the Safety of Life at Sea (SOLAS), vessels are
178 required to maintain continuous transmission of AIS signals throughout the year, except for specific
179 reasons permitted by regulations. Therefore, vessels theoretically maintain a high frequency of signal
180 transmission during navigation. Taking the year 2021 as an example, Fig. S 3 reveals a distinct bimodal
181 distribution of original AIS signals, with peaks occurring around 300 seconds and 2 hours. The peak of
182 around 300 seconds corresponds to the high-frequency interval for shore-based AIS equipment to receive
183 signals, while the peak of around 2 hours mainly originates from satellite AIS signals. Statistical analysis
184 shows that 99.6% of signal time intervals are within 8000 seconds. However, the total duration of these
185 AIS signal intervals accounts for only 16% of all AIS signals, indicating the presence of extremely long
186 consecutive signal intervals in the AIS data. This may be due to vessel docking for repairs or AIS
187 equipment malfunctions. To minimize uncertainty in emission calculations caused by these signals, this
188 study filters out signals with time intervals exceeding 7 days, which are not included in the emission
189 calculations.

190 Thirdly, for spatial distribution anomalies cleaning, AIS data distributed on land are filtered out.
191 Spatial distribution of the annual original AIS signal (Fig. S 4) revealed a significant number of signals
192 deviating from shipping routes near the 0° and 120° meridians, located over Asia, Europe, and Africa.
193 Further analysis indicated that such abnormal signal points are caused by misaligned field information
194 or data loss. To minimize the interference of these abnormal signals on emission calculations, this study

195 employs the following cleaning methods: 1) For ships matched by IMO codes, signals with speeds >50
196 knots or consecutive latitude-longitude spans >20° are removed; 2) For ships matched by MMSI codes,
197 signals with speeds >40 knots or latitude-longitude spans >8° are excluded; 3) Signals located on land
198 areas are excluded. Fig. S 4 simultaneously presents the spatial distribution of the cleaned AIS signals,
199 revealing that signals on land near the 0° and 120° meridians have been eliminated while retaining signals
200 on major navigable rivers in North America, South America, and Eurasia.

201 Fourthly, to ensure the reliability of ship technical parameter data matching, the AIS data are
202 subsequently aggregated and identified with IMO numbers and MMSI numbers. AIS data comprises
203 static AIS data and dynamic AIS data. Static AIS data include time, MMSI numbers, IMO numbers, etc.,
204 but do not contain latitude and longitude information. Dynamic AIS data contain MMSI numbers and
205 latitude and longitude information. This study integrates the static AIS data and dynamic AIS data by
206 matching their common MMSI numbers. It is found that approximately 84% of the MMSI numbers in
207 dynamic information could be matched with a unique valid seven-digit IMO number. However, some
208 ships may change their MMSI codes multiple times within a year. Data with MMSI code changes more
209 than 10 times are excluded from emission calculations.

210 **2.1.3 Engine power demand**

211 Engine power demand is crucial for emission calculations. For the main engine, its real-time output
212 power is related to the main engine load, which can be depicted in real-time by changes in the ship's
213 speed-over-ground obtained from AIS data. According to the propeller law, the main engine load factor
214 is the cube of the ratio of the ship's actual speed to its design speed (Liu et al., 2016). Additionally, some
215 studies indicate that factors such as draft, hydrological and weather conditions, and hull fouling also
216 influence the main engine load (Chen and Yang, 2024; Emmens et al., 2021; Fu et al., 2022). Regarding
217 draft factors, the (Jasper Faber, 2020) corrects the main engine load using real-time draft data from AIS.
218 However, draft fields in commercial AIS data are often manually recorded by crew members, leading to
219 low accuracy and a large number of zero values. As for hydrological and weather conditions, wind and
220 waves could increase engine power demand through friction and shear resistance. (Johansson et al., 2017)
221 adopts a method based on a real-time ship heading and weather field, which requires substantial
222 computational resources and introduces greater uncertainty by the weather field. Additionally, the

223 accumulation of micro- and macro-organisms on ship surfaces increases power demand to overcome
 224 resistance, and existing studies often use fixed parameters to correct the influence. This study introduces
 225 parameterization schemes to correct the influence of draft, weather, and hull fouling. Based on the ships'
 226 payload utilization calculation algorithm in (IMO, 2015), this study estimates the average drafts for
 227 different types of vessels, with specific values provided in Table S1. The correction coefficients for
 228 weather influences (η_w) are based on (Jasper Faber, 2020), also presented in Table S1. The correction
 229 coefficient for fouling influences (η_f) is set to 0.917. Specifically, the formula for calculating the real-
 230 time power of the main engine in SEIMv2.2 can be found in equation (5).

$$P_{ME,i,n} = P_{ref,i} \times LF_{i,n} = \frac{P_{ref,i} \times \left(\frac{D_i}{D_{ref,i}}\right)^{0.66} \times \left(\frac{v_{i,n}}{v_{ref,i}}\right)^3}{\eta_w \times \eta_f} \quad (5)$$

231 Where $P_{ref,i}$ represents the maximum engine output power (unit: kw) of the main engine of the
 232 ship i ; $LF_{i,n}$ represents the main engine load factor of the ship i at the n -th AIS signals in the sequence.
 233 D_i represents the average draft; $D_{ref,i}$ represents the designed draft; $v_{i,n}$ represents the speed-over-
 234 ground (unit: knot) of the ship i at the n -th AIS signals in the sequence; $v_{ref,i}$ represents the design
 235 speed (unit: knot) of ship i , obtained from the static technical profiles; $\eta_{w,i}$ represents the weather
 236 correction factor and $\eta_{f,i}$ represents the fouling correction factor, both of which are unitless.

237 For auxiliary engines and boilers' power demand, this study adopts the recommended values from the
 238 IMO Fourth and Third Greenhouse Gas Study reports. Due to the lack of information, this study did not
 239 consider the impact of other auxiliary devices on board, such as solar panels, wind sails, waste heat
 240 recovery systems, and carbon capture, utilization and storage (CCUS) systems, on vessel energy
 241 consumption. These systems are not significant contributors to overall vessel energy consumption
 242 currently (Dnv, 2022). However, with the ongoing trends of energy efficiency improvements, the impact
 243 of these systems on vessel energy utilization could be transformative in the future (Kersey et al., 2022).

244 **2.1.4 Emission factors**

245 The emission factors applied by SEIMv2.0 is mainly based on the Third IMO GHG Study (Smith,
 246 2014) as well as the National Standard for General Diesel Fuel of the People's Republic of China (Wang
 247 et al., 2021). In this study, we updated the emission factors based on the Forth IMO GHG Study (Jasper

248 Faber, 2020), and therefore accompanying technical modification. Firstly, emission factors of
 249 conventional air pollutants (SO₂, NO_x, PM_{2.5}, CO, HC) and GHGs (CO₂, CH₄, N₂O) were updated. CO₂,
 250 SO₂, and PM_{2.5} are considered typical species whose emission factors are highly dependent on the
 251 chemical component of fuels. Table. S2 represents the emissions factors based on fuel consumption for
 252 CO₂, SO₂, and PM_{2.5}. Energy-based emission factors are calculated based on fuel-based emission factors
 253 as well as specific fuel consumptions (SFC, unit: kwh/kg fuel), using Equation (6):

$$EF_e = EF_f \cdot SFC \quad (6)$$

254 SFC represents the fuel consumption per unit of work performed by a ship, mainly decided by the
 255 fuel calorific value (kwh/kg fuel) and engine efficiency (%). During the operation of ships, energy
 256 efficiency could be considered as a quadratic function of the load factor of the main engine, generally
 257 with the optimal load factor of 80%. Equation (7) is applied to calculate the SFC for main engines based
 258 on the SFC under the optimal operating condition (SFC_{base}) and main engine load of the ship i .

$$SFC_{ME,i} = SFC_{base,ME,i} \cdot (0.455 \cdot LF_i^2 - 0.71 \cdot LF_i + 1.28) \quad (7)$$

259 Generally, newer ships have a lower SFC_{base} than older ships due to the improvement of engine
 260 and auxiliary engine efficiency (Sou et al., 2022). The LNG fleet also has a lower SFC_{base} value than
 261 conventional fuel. SFC of auxiliary engines and boilers ($SFC_{AE|B,i}$) is not subject to the main engine load,
 262 so $SFC_{AE|B,base,i}$ is directly applied with no main engine load adjustment. Values of SFC_{base} are
 263 exhibited in Table. S 3.

264 Combining Table. S 2 and Equations (1), and (2), energy-based emission factors for the main
 265 engines of CO₂ and SO₂ as a function of the main engine load could be derived, as exhibited in Fig. S 1.
 266 It could be noted that although Marine Gas Oil (MGO) has a higher carbon content compared to Heavy
 267 Fuel Oil (HFO), its lower SFC results in a lower energy-based CO₂ emission factor. Fig. S 2 illustrates a
 268 comparison between two algorithms employed in SEIMv2.0, which utilizes uniform emission factors for
 269 all operational conditions, and SEIMv2.2, which incorporates load-dependent emission factors. We
 270 selected a typical oil tanker with dead-water tonnage of 7562 tons and examined its hourly carbon
 271 emissions from July 1 to July 15, 2019. It is evident that, at anchorage or berth, the hourly emissions

272 estimated by SEIMv2.2 are generally higher than or equal to those of the previous SEIMv2.0. When the
273 vessel is cruising, however, the overall emissions calculated by SEIMv2.2 are relatively lower compared
274 to SEIMv2.0. Emission factors of other air pollutants and GHGs in this study are shown in Table S 4 and
275 Table S 5.

276 **2.2 Data source and quality control**

277 **2.2.1 AIS data coverage**

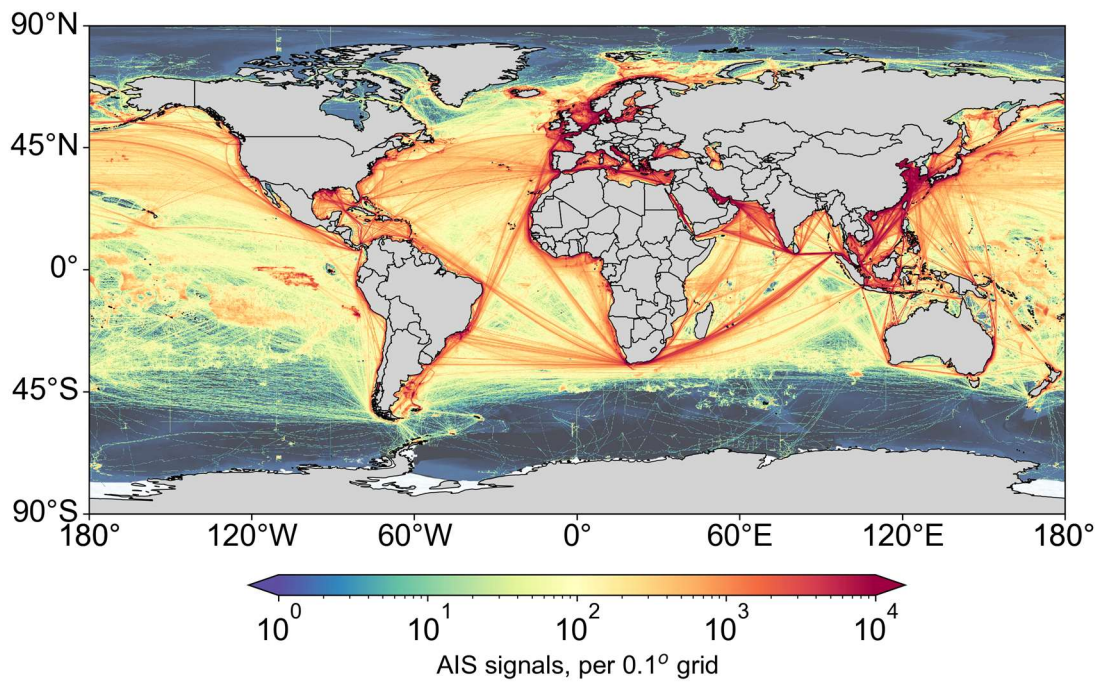
278 The AIS-observed data obtained in this study amounted to approximately 30 billion/year, while the
279 processed AIS signals after cleaning and interpolation averaged about 4-5 billion per year, with an
280 average annual operating time of approximately 5-7 million hours, as shown in Table 1. In comparison
281 to (Johansson et al., 2017), the AIS signal volume in this research is slightly lower, possibly due to
282 comprehensive quality control measures in data reduction and filtering, which removed a significant
283 number of signals with inadequate validity, abnormal time or spatial distribution, and insufficient
284 reliability. It can be observed that with the increasing prevalence of AIS equipment, the quantity of AIS
285 signals is on the rise. However, the operating time does not necessarily increase in proportion to the
286 signal quantity. The operating time decreased by 3.8% in 2020 compared to 2019 and increased by 4.5%
287 in 2021 compared to 2020, probably influenced by the pandemic,
288

289 **Table 1: Annual AIS signals and operating time after data cleaning**

Year	2013	2016	2017	2018	2019	2020	2021
AIS signals, billion	1.6	4.1	4.6	5.0	5.0	5.0	5.5
Operating time, million hour	225.8	578.5	643.6	700.9	693.8	667.3	697.6

290

291 Taking 2021 as an example, the spatial distribution of AIS signals after cleaning and time interpolation
 292 is illustrated in Fig. 2. The spatial coverage of cleaned AIS signals is extensive, with signals primarily
 293 concentrated along major shipping routes such as the coastal regions of East Asia, the Malacca Strait-
 294 Cape of Good Hope route, the Mediterranean, and the Black Sea routes, effectively depicting the
 295 trajectories of major shipping lanes.



296

297 **Figure 2: The spatial distribution of global AIS signals in 2021. Maps are made with Natural Earth.**

298

299 **2.2.2 Global fleet composition**

300 Table 2 presents the global fleet structure obtained through matching AIS data with STSD in 2021. This
 301 study covers 14 vessel types, including major cargo vessels, passenger ships, and fishing vessels, along

302 with a category labeled "others," comprising research vessels, rescue ships, and work vessels, among
303 others. Since the "others" category primarily consists of small coastal vessels, its contribution to
304 emissions is minor. It's important to note that United Nations Conference on Trade and Development
305 (UNCTAD) definition of "others" differs from this study's categorization. According to UNCTAD 2021
306 classification, other ships include liquefied petroleum gas carriers, liquefied natural gas carriers, parcel
307 (chemical) tankers, specialized tankers, reefers, offshore supply vessels, tugboats, dredgers, cruise ships,
308 ferries, and other non-cargo ships. Moreover, it should be noted that the fleet obtained in this study
309 comprises vessels with certain activity levels (annual AIS signals exceeding 10), whereas UNCTAD
310 statistics do not consider vessel activity. This discrepancy might lead to comparatively lower results in
311 this study.

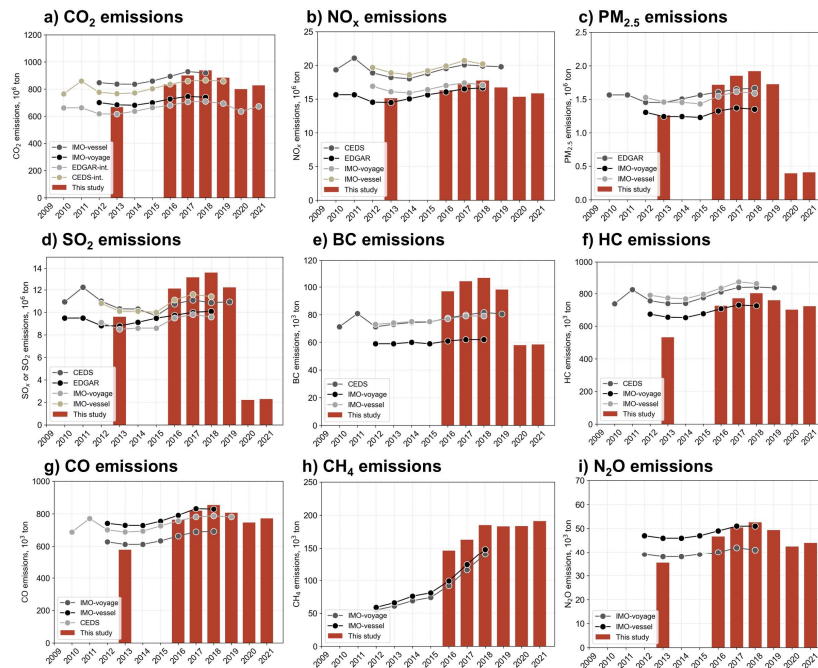
312 Overall, the discrepancies between the global fleet statistics in this study and those of UNCTAD are not
313 substantial. In terms of vessel numbers, this study reached 109.3 thousand in 2021, slightly higher than
314 UNCTAD's 101.4 thousand. The total deadweight tonnage amounts to 1989.9 million tons, slightly lower
315 than UNCTAD's 2136.2 million tons. Among the fleet obtained in this study, vessels matched by IMO
316 numbers reach 62.9 thousand, contributing 57.5% of vessel count and 95.4% of deadweight tonnage.
317 Vessels matched by MMSI numbers constitute a larger proportion in count (42.5%), yet make a smaller
318 contribution in deadweight tonnage (4.6%), predominantly consisting of fishing vessels (which
319 contribute 87.9% to the vessel count matched by MMSI numbers). There's a noticeable difference in the
320 quantity of general cargo ships and oil tankers. However, in terms of total tonnage, the container ships,
321 general cargo ships, bulk carriers, and oil tankers show no significant differences (below 10%) with
322 UNCTAD, ensuring the reliability of global ship emission calculations and emission structure analysis.
323

324 **Table 2: Comparison of the global fleet structure of this study and the UNCTAD statistics in 2021. The fleet**
 325 **analyzed in this study was filtered to include vessels with an annual AIS signal count greater than 10.**

Vessel type	Number of vessels, thousand				Total deadweight tonnage, million ton			
	This study			UNCTAD	This study			UNCTAD
	match with IMO number	match with MMSI number	total		match with IMO number	match with MMSI number	total	
Auto Carrier	0.8	0.1	0.8		15.3	0.9	16.2	
Bulk Carrier	11.1	0.6	11.7	12.3	842.3	27.6	869.9	913.2
Chemical Tanker	4.7	0.3	5.0		100.5	4.5	105.0	
Container	4.2	0.3	4.5	5.4	218.8	14.4	233.2	281.8
Cruise	0.2	0.1	0.2		0.1	0.0	0.1	
Fishing ship	5.1	40.8	45.8		4.0	5.8	9.7	
General Cargo	6.9	0.8	7.7	20.0	66.4	4.4	70.7	77.9
LNG	0.3	0.0	0.3		19.3	0.2	19.5	
LPG	1.2	0.1	1.2		19.0	0.8	19.9	
Miscellaneous	12.3	1.4	13.7		76.1	6.5	82.6	
Ocean Tug	7.0	0.9	7.9		13.4	1.6	15.0	
Oil Tanker	5.4	0.4	5.8	11.5	505.3	22.2	527.5	619.3
Reefer	0.5	0.0	0.5		3.5	0.2	3.7	
Ro Ro	3.0	0.6	3.6		11.8	1.7	13.5	
Others	0.5	0.0	0.5	52.2	3.1	0.0	3.1	243.9
Total	62.9	46.4	109.3	101.4	1899.1	90.8	1989.9	2136.2

326

328 3.1 Total global shipping emissions



329

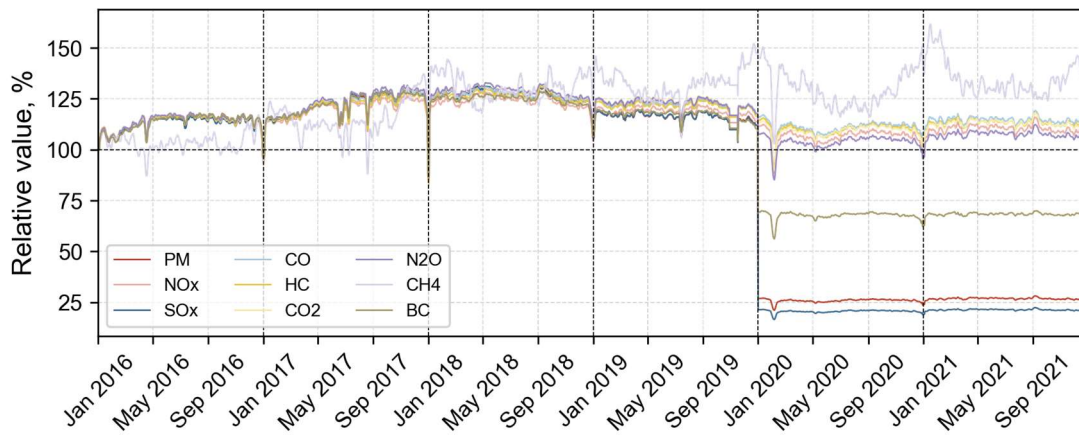
330 **Figure 3: Global trends in shipping emissions from 2010 to 2021.** Data source: IMO (Jasper Faber, 2020),
 331 where IMO-Voyage results were calculated based on a voyage-based method and IMO-Vessel on a vessel-based
 332 algorithm. Community Emissions Data System (Mcduffie et al., 2020); Emissions Database for Global
 333 Atmospheric Research (Crippa, 2021).

334 We established a multi-year global ship emissions inventory with temporal resolution of day and
 335 spatial resolution of 0.1° using the SEIM model for the years 2013 and 2016-2021. Figure 3 summarizes
 336 this study and open-source dataset of major atmospheric pollutants and greenhouse substances emitted
 337 by global shipping over the past decade. The ship emission calculation method employed in this research,
 338 which is AIS-based, aligns with those utilized in the EDGAR (Emissions Database for Global
 339 Atmospheric Research) inventory and the Fourth IMO GHG Study released in 2020, while the CEDS
 340 inventory is established based on a top-down fuel-based approach (Mcduffie et al., 2020).
 341 Methodologically, our study is more comparable to the research conducted by EDGAR and IMO, with
 342 the results from the CEDS inventory as a reference. It is important to note that the SEIM model has
 343 undergone two major version updates. The data of different versions are presented in Figure S3. Figure
 344 3 presents the integrated results for ease of comparison with other studies. Specifically, the results for
 345 2013 are based on SEIMv1.0, while those for 2016-2020 are based on SEIMv2.1 and those for 2021 are

346 based on SEIMv2.2. Due to slight differences between the two versions (Fig. S5), both of which include
347 data for 2020, the total emissions for 2020 in SEIMv2.2 were adjusted to match those in SEIMv2.1. The
348 growth rate for 2021 was kept consistent to ensure that the data for both versions align in 2020. In terms
349 of annual emission totals, this study's results show similarities in emission trends and total emissions
350 compared to well-known inventories such as EDGAR and IMO. For most species, this study's results
351 show higher annual growth rates compared to IMO and EDGAR studies. For instance, this study
352 estimates a 6.1% annual increase rate in global ship CO₂ emissions from 2016 to 2018, while IMO's
353 study indicates only a 1.4% annual increase for its "vessel-based" results and 0.9% for its "voyage-based"
354 results. In 2019 and 2020, influenced by international trade conflicts and the global pandemic, this study
355 estimates a 5.8% and 9.5% year-on-year decrease in global ship CO₂ emissions for 2019 and 2020,
356 respectively. In contrast, the year-on-year decrease rate estimated by EDGAR inventory is 2.1% and 8.4%
357 for 2019 and 2020, respectively. Differences between studies may stem from factors such as AIS data
358 quality, coverage of static information, and factors considered in emission calculations. In 2020, the
359 global implementation of the fuel-switching policy led to a significant reduction in the sulfur content of
360 ship fuel. According to SEIM, in 2020 relative to 2019, SO₂, PM_{2.5}, and BC emissions decreased by
361 81.9%, 77.2%, and 40.9%, respectively. In 2021, following the recovery in global trade demand after the
362 pandemic, this study estimates an increase of 3.5% in global ship CO₂ emissions compared with 2020,
363 while EDGAR inventory estimates an increase of 5.9%. However, the latest data on ship's atmospheric
364 pollutants from other inventories only extend to 2019, which is insufficient for comparing emission
365 results with this study.

366 3.2 Temporal evolutions

367 3.2.1 Daily shipping emissions



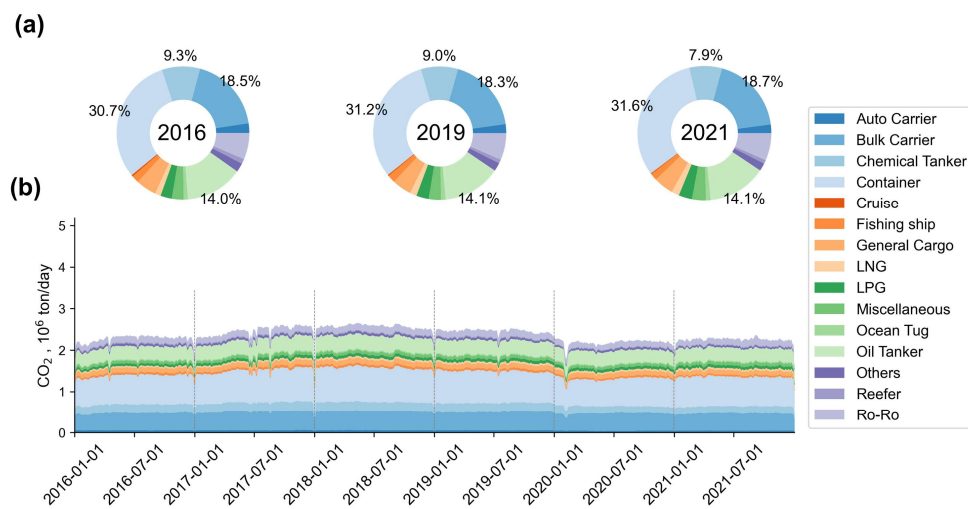
368

369 **Figure 4: Daily global shipping air pollutants and GHGs emissions from 2016 to 2021.** With January 1, 2016,
370 as the reference point, the five-day moving average of daily relative emissions is displayed.

371 To compare the magnitude of changes in emissions of various atmospheric pollutants and
372 greenhouse gases emitted by ships, Fig. 4 converts the daily ship emissions of 9 species into daily relative
373 quantities taking the emission levels on January 1, 2016, as the reference point. Figure 4 reveals that,
374 aside from occasional sharp declines or increases on certain dates, the daily variations in ship emissions
375 are generally stable. This suggests that the emission simulations by the SEIM model exhibit continuity
376 and stability. Ships typically cruise at constant speeds on high seas without significant diurnal or other
377 periodic variations, so global ship emissions do not exhibit pronounced daily or seasonal fluctuations.
378 Any anomalies such as sudden drops or spikes may be attributed to signal transmission anomalies in
379 equipment or meteorological factors. In 2019, the reduction in ship SO₂ emissions compared to 2018 was
380 slightly larger than that of other pollutants, probably attributed to the implementation of the domestic
381 emission control area policy within 12 nautical miles of the Chinese coast, one of the world's busiest
382 areas for shipping activities (Chen et al., 2017), which has also been demonstrated by Fig. 7c. From Fig.
383 4, finer temporal patterns can be observed, such as the gradual increase in emissions during the second
384 half of 2017 and the subsequent decrease in ship emissions in 2019 as trade conflicts intensified. In 2020,
385 the impact of the pandemic led to two phases of decline and recovery in global ship emissions. The 2020
386 global fuel-switching policy also led to a significant reduction in ship SO₂, PM_{2.5}, and BC emissions.
387 Despite the implementation of NECA policy from 2016 to 2021 (IMO, 2023), the decline in ship NO_x

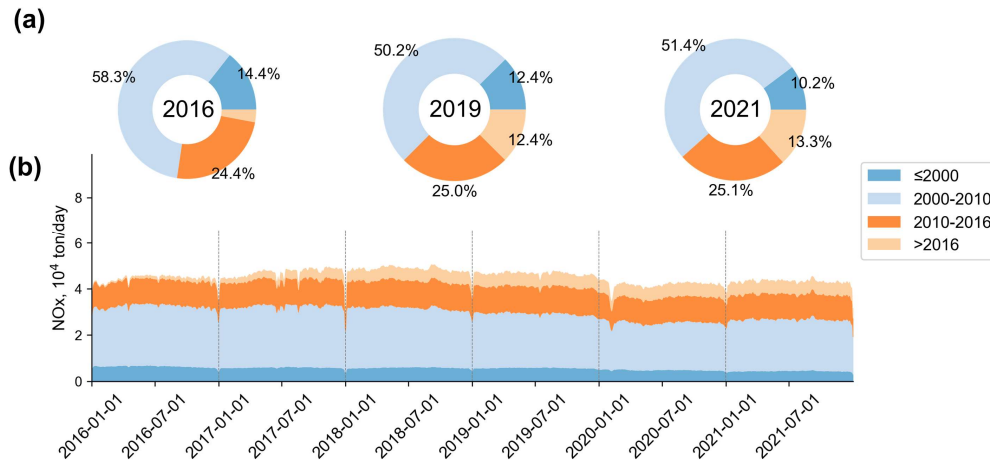
388 emissions is very slow, as shown in Fig. 4, which is due to the fact that the current fleet is still
 389 predominantly composed of ships built before 2016 (accounting for more than 85%, as shown in Figure
 390 6). The slow pace of fleet renewal makes it more challenging to achieve substantial reductions in NO_x
 391 emissions from ships currently. It is worth noting that CH₄ emissions exhibit relatively large daily
 392 changes and have been increasing throughout the six years. The primary source of CH₄ emissions is LNG
 393 ships. The daily fluctuations in ship CH₄ emissions are mainly due to variations in LNG ship activities.
 394 Although LNG ships are currently relatively few, their quantity is increasing as the demand for low-
 395 carbon ships grows steadily (Gronholm et al., 2021).

396 **3.2.2 Multi-dimensional structure**



397
 398 **Figure 5: Composition of global ship CO₂ emissions by vessel type from 2016 to 2021.** a) the percentage
 399 contribution of emissions by vessel type for the years 2016, 2019, and 2021; b) the five-day moving average of
 400 daily emissions for different vessel types.

401 Figure 5 displays the daily CO₂ emissions classified by vessel type. From 2016 to 2021, container
 402 ships, bulk carriers, and oil tankers consistently contributed the most, accounting for 31.6%, 18.7%, and
 403 14.1% of global ship CO₂ emissions in 2021, respectively. The contribution of container ships increased
 404 from 30.7% to 31.6% from 2016 to 2021. Overall, there were no significant changes in the composition
 405 of vessel types over the six years. Vessel types reflect the types of commodities transported by sea,
 406 indicating the relative stability of the global maritime cargo structure.



408

409 **Figure 6: Composition of global ship NO_x emissions by vessel construction year from 2016 to 2021.** a) the
 410 percentage contribution of emissions by vessels constructed in different periods for the years 2016, 2019, and 2021;
 411 b) the five-day moving average of daily emissions for vessels constructed in different periods.

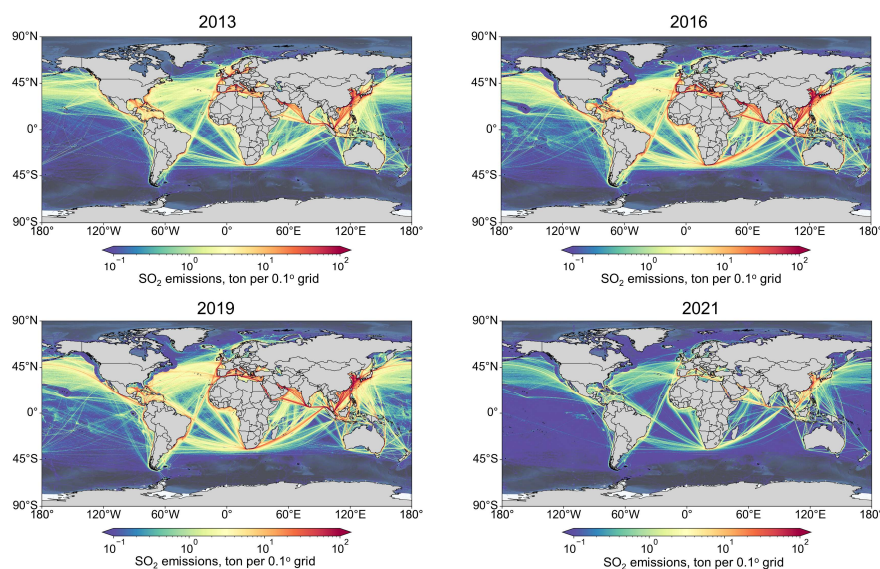
412 Figure 6 illustrates the daily NO_x emissions composed by the vessel construction period. The
 413 construction year of vessels determines the NO_x emission standards followed by their engine (IMO,
 414 2008). From 2016 to 2021, vessels complying with Tier I standards (built during the year 2000-2010)
 415 consistently contributed over 50% of ship NO_x emissions, while those complying with Tier II standards
 416 (built during the year 2010-2015) contributed approximately half of Tier I emissions. As the majority of
 417 ship NO_x emissions come from Tier I- and Tier II-standard vessels, global ship NO_x emissions are
 418 expected to remain at current levels in the short term without further control measures. However, it is
 419 noteworthy that the contribution of vessels over 20 years old (built-year ≤ 2000) to global ship NO_x
 420 emissions has gradually decreased, from 14.4% in 2016 to 10.2% in 2021. Meanwhile, the contribution
 421 of newly built vessels (built-year ≥ 2016) to global ship NO_x emissions has steadily increased from
 422 3.5% in 2019 to 13.3% in 2021.

423 3.3 Spatial characteristics

424 3.3.1 High-resolution patterns

425 Based on latitude and longitude coordinates in AIS signals, the ship emissions dataset was spatially
 426 aggregated into grids, resulting in the global spatial distribution of ship emissions. Figure 7 depicts the
 427 SO₂ emissions from global ships in $0.1^\circ \times 0.1^\circ$ grids. The regions with high intensity of ship SO₂
 428 emissions include East Asia, South Asia, Europe, the Persian Gulf, the Mediterranean, and the western
 429 coast of Europe. The intensive ship emissions along major global shipping routes are clearly visible, such

430 as the routes connecting East Asia through the Malacca Strait, the Suez Canal, and the Strait of Hormuz
 431 to Western European countries (the "Europe-Middle East-Far East route"), the Strait of Gibraltar, the
 432 Strait of Hormuz, and the critical passage connecting the Pacific and Atlantic Oceans, the Panama Canal,
 433 among others. Comparing the spatial distribution of ship SO₂ emissions in different years, noticeable
 434 reductions in emissions are observed in ECAs such as North America, the Gulf of Mexico, the North Sea,
 435 and the Baltic Sea comparing the ship SO₂ emissions distribution in 2013 and 2016. A significant
 436 reduction in emissions is also observed in the Domestic Emission Control Area (DECA) comparing the
 437 ship SO₂ emissions distribution in 2016 and 2019. In 2021, the implementation of the global low-sulfur
 438 fuel policy resulted in a significant overall reduction in ship SO₂ emissions spatially compared with 2019.
 439 The spatial distribution of ship SO₂ emissions in different years demonstrates that the SEIM v2.2
 440 effectively responds to SO₂ emission control policies.

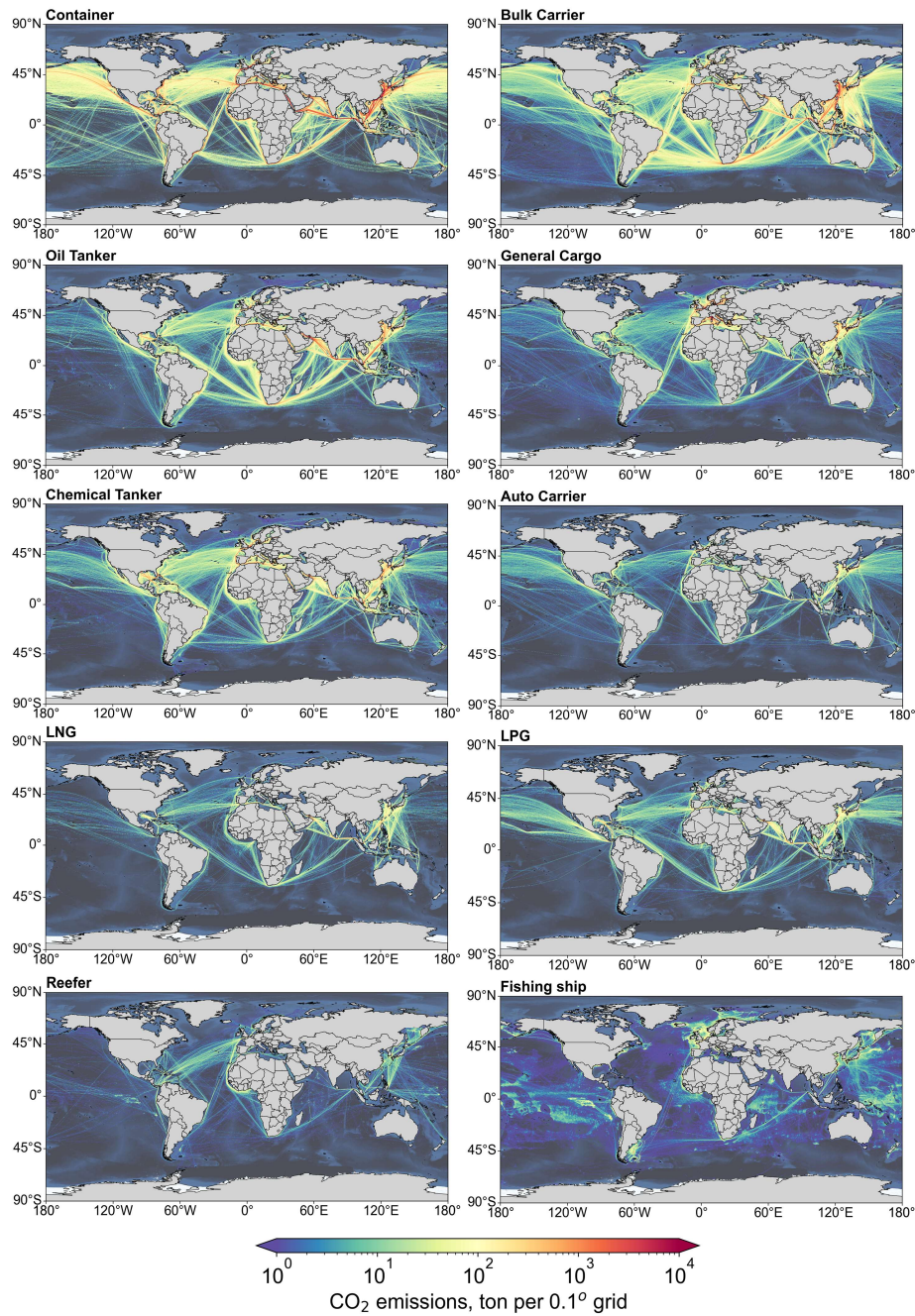


441
 442 **Figure 7: Spatial distribution of global ship SO₂ emissions in different years**

443 3.3.2 Spatial disparities of vessel composition

444 Distinct disparities in spatial distribution are evident between freight vessels and non-freight
 445 vessels in Fig. 8. Emissions from container ships, bulk carriers, and oil tankers are concentrated in major
 446 international shipping lanes. In contrast, emissions from non-transport vessels such as fishing vessels are
 447 more widely distributed in non-lane open sea areas. According to this study, in 2021, fishing vessels
 448 contributed 1.6% to global ship CO₂ emissions, with their emissions mainly concentrated in the North
 449 Sea, Baltic Sea, Yellow Sea, and South Pacific. In recent years, studies have utilized fine satellite data to

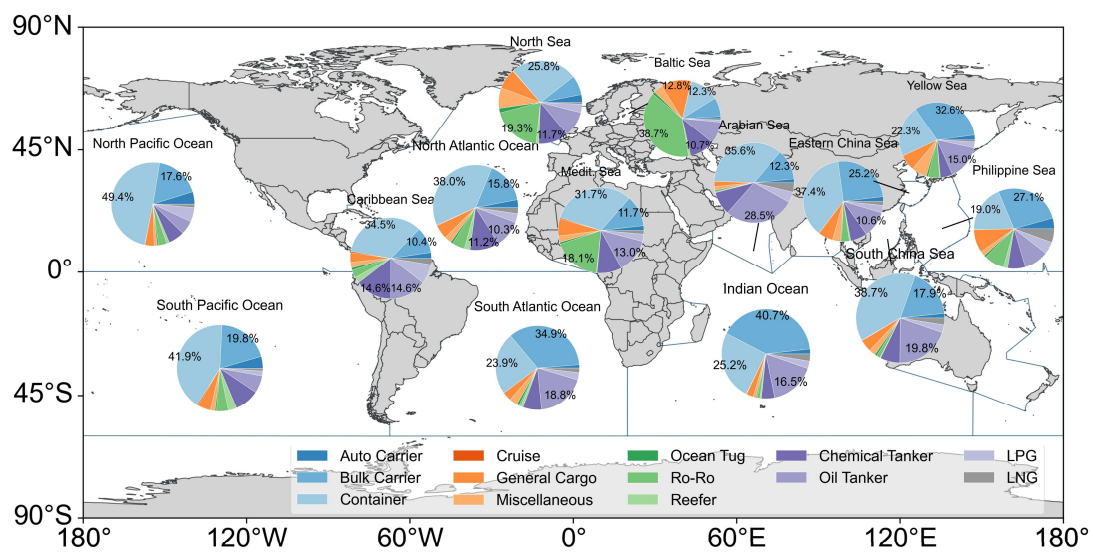
450 reveal significant fishing vessel activities that had not been publicly tracked worldwide (Paolo et al.,
 451 2024). The emissions from those fishing vessels remain unknown. Therefore, the emissions from fishing
 452 vessels presented in this study should be considered highly uncertain and are not discussed in the
 453 following sections.



454

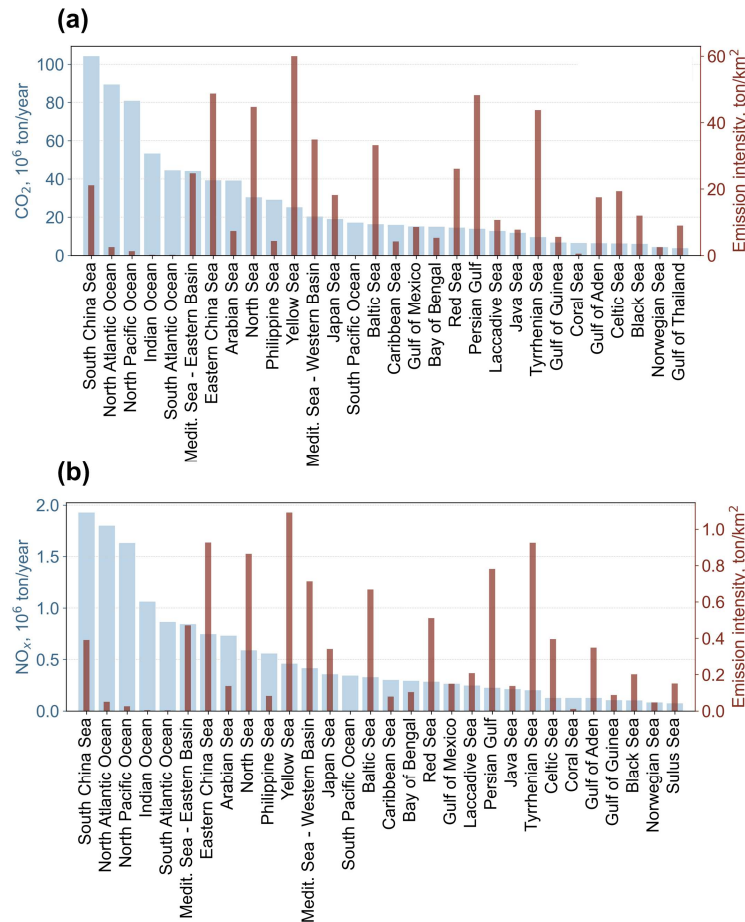
455 **Figure 8: Spatial distribution of CO₂ emissions from different types of vessels in 2021**

456 The spatial distribution of emissions varies across different vessel types, leading to disparities in the
 457 composition of vessel types in different maritime regions. The division of global maritime regions is
 458 based on the International Hydrographic Organization (IHO) standards (<https://iho.int/>). Figure 9
 459 illustrates the composition of vessel types in the top 14 regions with the highest CO₂ emissions globally
 460 in 2021, with their combined emissions accounting for almost 80% of the total global emissions. In the
 461 pie charts for each region, vessel types contributing over 10% of emissions are labeled. It is observed
 462 that container ships contribute significant emissions in the North Pacific Ocean, South China Sea, and
 463 East China Sea, accounting for 49.4%, 37.4%, and 38.7% respectively, well above the global average
 464 (31.6%). Regions with high contributions from bulk carriers are mainly distributed in the southern
 465 hemisphere, such as the Indian Ocean (40.7%) and South Atlantic (34.9%). Ro-Ro vessels exhibit high
 466 emissions proportions near Europe, with percentages of 38.7% in the Baltic Sea, 19.3% in the North Sea,
 467 and 18.1% in the Mediterranean. Oil tankers contribute 28.5% of emissions in the Arabian Sea, probably
 468 attributed to countries like Saudi Arabia and Iran, rich in oil and gas resources, generating substantial
 469 shipping emissions during exports to other countries.



470
 471 **Figure 9: Ship CO₂ emissions composition in different maritime regions globally in 2021 (excluding fishing**
 472 **ships and others)**

473 **3.3.3 Emission intensity**



474
 475 **Figure 10: Global ship (a) CO₂ and (b) NO_x emission and emission intensities in different maritime regions**
 476 **in 2021**

477 Since the significant differences in the area of $0.1^\circ \times 0.1^\circ$ grids at different latitudes, ship emissions
 478 within each grid are standardized into emission intensity, i.e., emissions per unit area (unit: ton/km²).
 479 Taking ship CO₂ emissions as an example, Fig. 10 illustrates the total ship CO₂ emissions and emission
 480 intensity in major maritime regions in 2021. The top 30 maritime regions with the highest CO₂ and NO_x
 481 emissions, accounting for approximately 96% of the total global ship emissions, are listed and arranged
 482 in descending order of total emissions. It is important to note that the South/North Pacific, South/North
 483 Atlantic, and Indian Ocean cover a vast area (about 75% of the total maritime area), most of which have
 484 little or no ship navigation. Calculating the total average emission intensity for these regions would
 485 weaken their significance, so they are not discussed here. Among other maritime regions, the South China
 486 Sea has the highest total ship CO₂ and NO_x emissions. As a vital route for maritime trade between East
 487 Asia Europe and Africa, the South China Sea exhibits prominent ship traffic density globally.

488 Additionally, the Eastern Mediterranean Basin, the Arabian Sea, the East China Sea, the Philippine Sea,
489 and the North Sea also have relatively significant total emissions. Generally, maritime regions with high
490 CO₂ emissions also have relatively high NO_x emissions. Although the order of maritime regions with
491 lower emissions differs slightly, overall consistency is observed. There are significant differences
492 between maritime regions with high emissions and those with high emission intensity. The top five
493 maritime regions with the highest ship CO₂ emission intensity are the Yellow Sea, the Persian Gulf, the
494 East China Sea, the North Sea, and the Tyrrhenian Sea. The top five for NO_x emission intensity are also
495 the same maritime regions. These regions are coastal areas or busy maritime routes with intensive ship
496 emissions, which warrants attention in environmental management in the future.

497 **4 Data Availability**

498 Shipping emission data described in this manuscript can be accessed at Zenodo under
499 <https://zenodo.org/records/11069531> (Wen et al., 2024).

500 **5 Conclusions**

501 Utilizing the SEIM model, we developed a high-resolution ship emission inventory covering the
502 period from 2013 to 2016-2021 globally, encompassing 5 atmospheric pollutants (NO_x, SO₂, PM_{2.5}, CO,
503 HC) and 4 greenhouse gases (CO₂, CH₄, N₂O, BC). With a temporal resolution of day and spatial
504 resolution of 0.1° × 0.1°, our inventory revealed novel insights into global ship emission characteristics.

505 In terms of annual emissions, our inventory exhibits consistency in temporal trends and emission
506 magnitudes compared to mainstream inventory datasets including EDGAR, CEDS, and IMO. According
507 to this study and the global anthropogenic emission inventory by (Hoesly Rachel, 2024), ship emissions
508 contributed 12.3% of SO₂, 14.0% of NO_x, and 2.5% of CO₂ to global anthropogenic emissions in 2019,
509 and 3.2% of SO₂, 14.2% of NO_x, and 2.3% of CO₂ to global anthropogenic emissions in 2021. Over the
510 years, ship CO₂, NO_x, CO, HC, and N₂O emissions showed a declining trend due to the impacts of the
511 2019 trade conflict (year-on-year decrease rate 5.4%-6.2%) and the 2020 pandemic (year-on-year
512 decrease rate 7.4%-13.8%), with a subsequent rebound in 2021 as international trade increased (year-on-
513 year increase rate 3.1%-3.6%). SO_x, PM, and BC emissions were significantly influenced by gradually

514 implemented ECA policies and the 2020 low-sulfur fuel-switching policy. SO_x and PM emissions in
515 2021 were 80.9% and 76.0% of those in 2019, and BC emissions were 38.7% of those in 2019. CH₄
516 emissions exhibited an increasing trend over the years, growing by 43.5% in 2021 compared to 2016.

517 Regarding emission composition, container ships consistently constituted the primary source of
518 global ship CO₂ emissions, contributing over 30% annually and steadily increasing, followed by bulk
519 carriers, oil tankers, and chemical tankers. The proportion of emissions contributed by new ships
520 increased annually from 3.5% in 2016 to 13.3% in 2021. However, Tier I and Tier II ships still dominate
521 ship NO_x emissions. Currently, Tier III standards only apply to vessels operating in North American
522 Emission Control Areas. Achieving a significant reduction in global ship NO_x emissions still requires
523 extensive advancements in ship engine technology and follow-up regulatory measures worldwide.

524 As for spatial characteristics, ship emissions were particularly significant in East Asia, South Asia,
525 and Europe, with busy shipping routes such as the Western Europe-Middle East-Far East route, the Strait
526 of Malacca, the Strait of Gibraltar, the Strait of Hormuz, and the Panama Canal showing the highest
527 emission intensities. The regions with the highest CO₂ and NO_x ship emission intensities were the Yellow
528 Sea, the Persian Gulf, the East China Sea, the North Sea, and the Tyrrhenian Sea. These are not only
529 areas with the highest emission intensity but also coastal regions with dense populations and ecosystems
530 vulnerable to pollution. This suggests that these regions should be prioritized in environmental
531 management efforts for improving air quality, protecting marine ecosystems, and climate mitigation.
532 Furthermore, influenced by the types of commodities transported and the countries involved in trade,
533 significant differences in ship emission characteristics exist across different regions. SEIM enables the
534 analysis of the heterogeneity of spatial distributions of ship emissions. In terms of vessel type
535 composition, container ships significantly exceeded the global average in ship CO₂ emissions
536 contributions in the North Pacific, East China Sea, and South China Sea. Regions with high proportions
537 of emissions from bulk carriers were mainly located in the Southern Hemisphere, such as the Indian
538 Ocean, South Pacific, and South Atlantic. Emissions from oil tankers were high in the Arabian Sea and
539 the Persian Gulf. The findings on the spatial heterogeneity of global ship emissions offer insights into
540 region-specific management. In addition, since many high-emission regions include transboundary areas,
541 such as the South China Sea and the Mediterranean, where maritime traffic connects multiple countries.,
542 effective mitigation in these regions will require international cooperation.

543 Although the complex quality control processes employed in this study, uncertainties still persist in
544 the aspects of AIS data accuracy, emission factors and so on. In the next steps, more work should be
545 done to reduce the uncertainties in bottom-up ship emission evaluation model, including integrating latest
546 methods and multi-source data to improve the accuracy of AIS data quality control, gathering more
547 studies on recent ship emission factors to cover more ship size and operating status, as well as involving
548 multiple data sources such as satellite data to validate the results. Overall, SEIM offers a globally multi-
549 year, high spatiotemporal resolution ship emission inventory that provides reliable and detailed data,
550 which could support foundational research across disciplines such as atmospheric science, environmental
551 science, and geoscience. Meanwhile, this dataset could also provide scientific support for facilitating
552 shipping emission mitigation in the future.

553 **Acknowledgments**

554 This work was supported by the National Natural Science Foundation of China (grant nos. 42325505),
555 National Key Research and Development Program of China (No. 2023YFC3705604 and No.
556 2022YFC3704200), and China Postdoctoral Science Foundation (No. 2023M730142).

557 **Author contributions**

558 W.Y. and X.W designed the research and wrote the manuscript, H.L. reviewed and revised the
559 manuscript, and T.H. contributed to the modelling. Z.L. and Z.L. contributed to data analysis. K.H. and
560 H.L. provided insights into the research design. All authors contributed to the writing. We also thank
561 Harvard-China Project on Energy, Economy and Environment and Professor Chris P. Nielsen from
562 Harvard University, for his suggested revisions to this manuscript.

563 **Competing interests**

564 The authors declare no competing interests.

565 **References**

- 566 Browse, J., Carslaw, K. S., Schmidt, A., and Corbett, J. J.: Impact of future Arctic shipping on high-
567 latitude black carbon deposition, *Geophysical Research Letters*, 40, 4459-4463,
568 <https://doi.org/10.1002/grl.50876>, 2013.
- 569 Chen, D., Wang, X., Li, Y., Lang, J., Zhou, Y., Guo, X., and Zhao, Y.: High-spatiotemporal-resolution
570 ship emission inventory of China based on AIS data in 2014, *Science of The Total Environment*, 609,
571 776-787, 10.1016/j.scitotenv.2017.07.051, 2017.
- 572 Chen, D., Fu, X., Guo, X., Lang, J., Zhou, Y., Li, Y., Liu, B., and Wang, W.: The impact of ship emissions
573 on nitrogen and sulfur deposition in China, *Science of The Total Environment*, 708, 134636,
574 <https://doi.org/10.1016/j.scitotenv.2019.134636>, 2020.
- 575 Chen, X. and Yang, J.: Analysis of the uncertainty of the AIS-based bottom-up approach for estimating
576 ship emissions, *Marine Pollution Bulletin*, 199, 115968,
577 <https://doi.org/10.1016/j.marpolbul.2023.115968>, 2024.
- 578 Corbett, J. J., Fischbeck, P. S., and Pandis, S. N.: Global nitrogen and sulfur inventories for oceangoing
579 ships, *Journal of Geophysical Research: Atmospheres*, 104, 3457-3470, 10.1029/1998jd100040, 1999.
- 580 Crippa, M., Guizzardi, D., Solazzo, E., Muntean, M., Schaaf, E., Monforti-Ferrario: GHG emissions of
581 all world countries - 2021 Report, Luxembourg, 2021.
- 582 Development, t. U. N. C. o. T. a.: Review of Maritime Transport, 2023.
- 583 Diamond, M. S.: Detection of large-scale cloud microphysical changes within a major shipping corridor
584 after implementation of the International Maritime Organization 2020 fuel sulfur regulations, *Atmos.*
585 *Chem. Phys.*, 23, 8259-8269, 10.5194/acp-23-8259-2023, 2023.
- 586 DNV: Maritime Forecast to 2050, 2022.
- 587 Emmens, T., Amrit, C., Abdi, A., and Ghosh, M.: The promises and perils of Automatic Identification
588 System data, *Expert Systems with Applications*, 178, 114975,
589 <https://doi.org/10.1016/j.eswa.2021.114975>, 2021.
- 590 Endresen, O., Sorgard, E., Sundet, J. K., Dalsoren, S. B., Isaksen, I. S. A., Berglen, T. F., and Gravir, G.:
591 Emission from international sea transportation and environmental impact, *Journal of Geophysical*
592 *Research-Atmospheres*, 108, 10.1029/2002jd002898, 2003.
- 593 Eyring, V., Isaksen, I. S. A., Bernsten, T., Collins, W. J., Corbett, J. J., Endresen, O., Grainger, R. G.,
594 Moldanova, J., Schlager, H., and Stevenson, D. S.: Transport impacts on atmosphere and climate:
595 Shipping, *Atmospheric Environment*, 44, 4735-4771, 10.1016/j.atmosenv.2009.04.059, 2010.
- 596 Fu, M., Liu, H., Jin, X., and He, K.: National- to port-level inventories of shipping emissions in China,
597 *Environmental Research Letters*, 12, 10.1088/1748-9326/aa897a, 2017.
- 598 Fu, X., Chen, D., Guo, X., Lang, J., and Zhou, Y.: Improving the estimation of ship emissions using the
599 high-spatiotemporal resolution wind fields simulated by the Weather Research and Forecast model: A
600 case study in China, *Journal of Industrial Ecology*, 26, 1871-1881, <https://doi.org/10.1111/jiec.13278>,
601 2022.
- 602 Gronholm, T., Makela, T., Hatakka, J., Jalkanen, J. P., Kuula, J., Laurila, T., Laakso, L., and Kukkonen,
603 J.: Evaluation of Methane Emissions Originating from LNG Ships Based on the Measurements at a
604 Remote Marine Station, *Environ Sci Technol*, 55, 13677-13686, 10.1021/acs.est.1c03293, 2021.
- 605 Hoesly Rachel, S. S.: CEDS v_2024_04_01 Release Emission Data (v_2024_04_01) Zenodo [dataset],
606 <https://doi.org/10.5281/zenodo.10904361>, 2024.

607 IMO: Emission Control Areas (ECAs) designated under MARPOL Annex VI.
608 IMO: Amendments to the technical code on control of emission of nitrogen oxides from marine diesel
609 engines, 2008.
610 IMO: Further technical and operational measures for enhancing the energy efficiency of international
611 shipping, 2015.
612 Jalkanen, J. P., Johansson, L., Kukkonen, J., Brink, A., Kalli, J., and Stipa, T.: Extension of an assessment
613 model of ship traffic exhaust emissions for particulate matter and carbon monoxide, *Atmospheric*
614 *Chemistry and Physics*, 12, 2641-2659, 10.5194/acp-12-2641-2012, 2012.
615 Jasper Faber, S. H., Shuang Zhang, Paula Pereda, Bryan Comer: Forth IMO Greenhouse gas study,
616 London, 2020.
617 Johansson, L., Jalkanen, J.-P., and Kukkonen, J.: Global assessment of shipping emissions in 2015 on a
618 high spatial and temporal resolution, *Atmospheric Environment*, 167, 403-415,
619 10.1016/j.atmosenv.2017.08.042, 2017.
620 Kersey, J., Popovich, N. D., and Phadke, A. A.: Rapid battery cost declines accelerate the prospects of
621 all-electric interregional container shipping, *Nature Energy*, 7, 664-674, 10.1038/s41560-022-01065-y,
622 2022.
623 Kramel, D., Muri, H., Kim, Y., Lonka, R., Nielsen, J. B., Ringvold, A. L., Bouman, E. A., Steen, S., and
624 Strømman, A. H.: Global Shipping Emissions from a Well-to-Wake Perspective: The MariTEAM Model,
625 *Environmental Science & Technology*, 55, 15040-15050, 10.1021/acs.est.1c03937, 2021.
626 Liu, H., Fu, M., Jin, X., Shang, Y., Shindell, D., Faluvegi, G., Shindell, C., and He, K.: Health and climate
627 impacts of ocean-going vessels in East Asia, *Nature Climate Change*, 6, 1037-1041,
628 10.1038/nclimate3083, 2016.
629 Liu, H., Yi, W., Jalkanen, J.-P., Luo, Z., Majamäki, E., Matthias, V., Moldanová, J., Shi, Z., and He, K.:
630 Atmospheric impacts and regulation framework of shipping emissions: achievements, challenges and
631 frontiers, *Fundamental Research*, <https://doi.org/10.1016/j.fmre.2024.02.013>, 2024.
632 Luo, Z., He, T., Yi, W., Zhao, J., Zhang, Z., Wang, Y., Liu, H., and He, K.: Advancing shipping NO_x
633 pollution estimation through a satellite-based approach, *PNAS Nexus*, pgad430,
634 10.1093/pnasnexus/pgad430, 2023.
635 Luo, Z., Lv, Z., Zhao, J., Sun, H., He, T., Yi, W., Zhang, Z., He, K., and Liu, H.: Shipping-related
636 pollution decreased but mortality increased in Chinese port cities, *Nature Cities*, 1, 295-304,
637 10.1038/s44284-024-00050-8, 2024.
638 McDuffie, E. E., Smith, S. J., O'Rourke, P., Tibrewal, K., Venkataraman, C., Marais, E. A., Zheng, B.,
639 Crippa, M., Brauer, M., and Martin, R. V.: A global anthropogenic emission inventory of atmospheric
640 pollutants from sector- and fuel-specific sources (1970–2017): an application of the Community
641 Emissions Data System (CEDS), *Earth System Science Data*, 12, 3413-3442, 10.5194/essd-12-3413-
642 2020, 2020.
643 Paolo, F. S., Kroodsma, D., Raynor, J., Hochberg, T., Davis, P., Cleary, J., Marsaglia, L., Orofino, S.,
644 Thomas, C., and Halpin, P.: Satellite mapping reveals extensive industrial activity at sea, *Nature*, 625,
645 85-91, 10.1038/s41586-023-06825-8, 2024.
646 Smith, T. W. P. J., J. P.; Anderson, B. A.; Corbett, J. J.; Faber, J.; Hanayama: Third IMO GHG Study,
647 London, 2014.

648 Sou, W. S., Goh, T., Lee, X. N., Ng, S. H., and Chai, K.-H.: Reducing the carbon intensity of international
649 shipping – The impact of energy efficiency measures, *Energy Policy*, 170, 10.1016/j.enpol.2022.113239,
650 2022.

651 Stephenson, S. R., Wang, W., Zender, C. S., Wang, H., Davis, S. J., and Rasch, P. J.: Climatic Responses
652 to Future Trans-Arctic Shipping, *Geophys Res Lett*, 45, 9898-9908, 10.1029/2018GL078969, 2018.

653 Wang, X., Yi, W., Lv, Z., Deng, F., Zheng, S., Xu, H., Zhao, J., Liu, H., and He, K.: Ship emissions
654 around China under gradually promoted control policies from 2016 to 2019, *Atmospheric Chemistry and
655 Physics*, 21, 13835-13853, 10.5194/acp-21-13835-2021, 2021.

656 Wen, Y., Xiaotong, W., Tingkun, H., Huan, L., Luo, Z., and Kebin, H.: Global shipping emissions for
657 the years 2013 and 2016-2021, Zenodo [dataset], 10.5281/zenodo.10869014, 2024.

658 Yuan, T., Song, H., Wood, R., Wang, C., Oreopoulos, L., Platnick, S. E., von Hippel, S., Meyer, K.,
659 Light, S., and Wilcox, E.: Global reduction in ship-tracks from sulfur regulations for shipping fuel,
660 *Science Advances*, 8, eabn7988, 10.1126/sciadv.abn7988, 2022.

661 Zhang, C., Shi, Z., Zhao, J., Zhang, Y., Yu, Y., Mu, Y., Yao, X., Feng, L., Zhang, F., Chen, Y., Liu, X.,
662 Shi, J., and Gao, H.: Impact of air emissions from shipping on marine phytoplankton growth, *Science of
663 The Total Environment*, 769, 145488, <https://doi.org/10.1016/j.scitotenv.2021.145488>, 2021.

664 Zhang, Q., Wan, Z., Hemmings, B., and Abbasov, F.: Reducing black carbon emissions from Arctic
665 shipping: Solutions and policy implications, *Journal of Cleaner Production*, 241,
666 10.1016/j.jclepro.2019.118261, 2019.

667

668